

Photochemical fabrication of silver nanostructures at the solid–liquid interface using a recyclable photosensitized reduction process†

Masanori Sakamoto,^a Sung Sik Kim,^{ab} Hirotohi Furusho^c and Tetsuro Majima^{*a}

Received 3rd September 2009, Accepted 6th October 2009

First published as an Advance Article on the web 11th November 2009

DOI: 10.1039/b917981j

Photochemical synthesis of metal nanostructures through photosensitized reduction of metal sources is a powerful method in a wide variety of environments, because light can selectively promote the desired reaction without damaging the surrounding environment. A drawback of the method is that most organic photosensitizers are disposable and consumed during the photochemical reactions and as a consequence a much larger amount of photosensitizer than that of the metal source is usually required, and therefore, the photosensitized reduction method is wasteful in terms of the sensitizer. In the present work, we propose a new photochemical synthetic method using a recyclable photosensitizer and applied it to fabricate Ag nanostructures at the solid–liquid interface. The photosensitized reduction of Ag ion at the solid–liquid interface resulted in the formation of unique Ag nanostructures (nanowires or plates) without the use of templates or stabilizing agents. The relation between the morphology and several external contributing factors, such as solvent polarity and interaction between the substrate and crystal phase, was discussed.

Introduction

Numerous researches have been conducted on noble-metal nanostructures due to their excellent optical, electronic and chemical properties, as well as their promising applications in the fields of nanoelectronics and sensing, and in the manufacture of optical devices and fluorescent probes.^{1–5} During the past decades, various synthetic strategies have been developed to control the sizes, shapes and topology of the nanostructures.^{6–12} Among them, photochemical synthesis of metal nanostructures through the photosensitized reduction of metal sources is a powerful method in a wide variety of environments, because the light can selectively promote the desired reaction without damaging the surrounding environment.^{12–20}

A drawback of the method is that most organic photosensitizers are consumed during the photochemical reactions. Due to this drawback a larger amount of photosensitizer than that of the metal source is usually required. Therefore, the photosensitized reduction method is wasteful.

Previously, we developed a recyclable photosensitization system driven by the two-colour two-photon excitation, which can overcome the drawback of use of organic photosensitizers (see Experimental section and Scheme 1 for the mechanism).²¹

In the present study, we applied the recyclable photosensitization system to fabricate metal nanostructures at the solid–liquid interface and investigated the morphologies of the generated nanostructures.

Crystal growth at the solid–liquid interface is an interesting process that helps us to understand the effect of external environmental factors (especially the type of interfaces) on the nanostructures. Solid–liquid interfaces are used for the fabrication of nanostructures in various crystal growth processes under natural as well as laboratory conditions.^{22–30} Furthermore, the structure and crystallographic orientation of inorganic crystals on a self-assembled monolayer are reported to reflect the interaction between the crystal phases and an organic monolayer.^{22–26,29–30} A prevalent method to aid inorganic crystal growth at the solid–liquid interface is the gentle chemical reduction of inorganic ions or electrochemical deposition; however, the photosensitized reduction method is also favorable owing to the reaction selectivity. The combination of photosensitization and nanostructure formation at the solid–liquid interface would expand the possibility of photochemical approaches for constructing a wide variety of metal nanostructures.

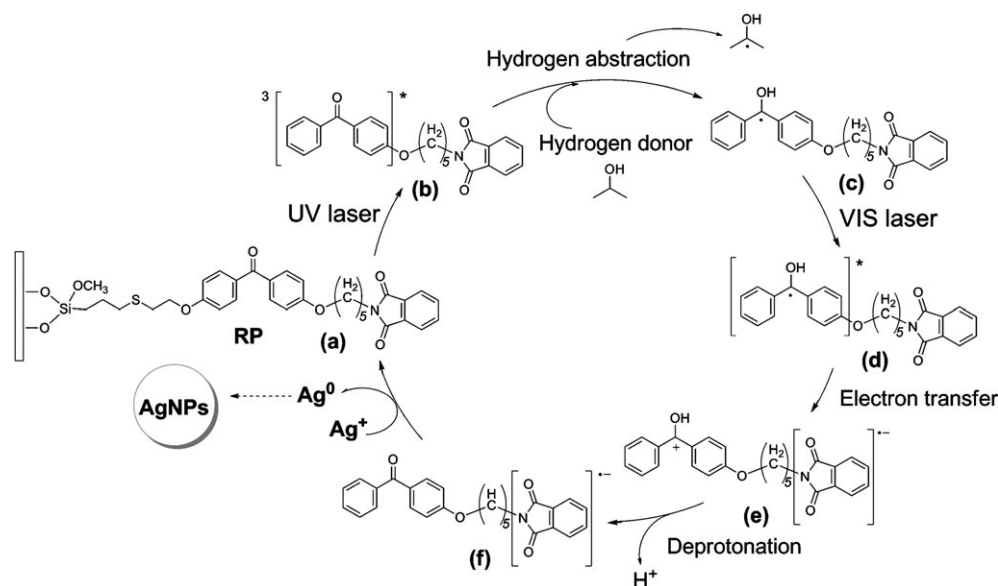
In this work Ag nanostructures were successfully fabricated using the recyclable photosensitization at the interface between an aqueous–alcoholic solution and an Si wafer covered with coordinated organic molecules. The morphologies of these nanostructures were characterized using transmission electron microscopy (TEM) and scanning electron microscopy (SEM). By fabricating the nanostructures at the solid–liquid interface, unique structures (nanowires or plates) can be obtained without using templates or stabilizing agents. Interestingly, depending on the solvent polarity and surface-modified substrate, dramatic changes were observed in the morphology of the nanostructures. The relationship between the external

^a The Institute of Scientific and Industrial Research (SANKEN), Osaka University, Mihogaoka 8-1, Ibaraki, Osaka 567-0047, Japan. E-mail: majima@sanken.osaka-u.ac.jp

^b Department of Chemistry, Chonbuk National University, Chonju 561-756, Korea

^c Research Center for Ultra-High Voltage Electron Microscopy, Osaka University, Mihogaoka, Ibaraki, Osaka, 567-0047, Japan

† Electronic supplementary information (ESI) available: EDS analysis of Ag nanostructure fabricated on substrate, SEM image of Ag nanostructure fabricated by single UV irradiation on substrate **I**, AFM image of Si wafer and organic surface, and measurement of contact angle of aqueous alcoholic solution on substrates. See DOI: 10.1039/b917981j



Scheme 1 Mechanism of recyclable photosensitization.

environmental factors (*i.e.*, solvent polarity and interaction between the substrate and Ag crystal phase) and the nanostructure formation were discussed.

Experimental

Mechanism of recyclable photosensitizer

The recyclable photosensitizer (RP) was designed for the photosensitized reduction of Ag ion at the solid–liquid interface. The mechanism of recyclable photosensitization is illustrated in Scheme 1.²¹ In the first step, the 4-methoxybenzophenone (MeOBP) chromophore of the RP is excited by UV light to generate MeOBP in the triplet excited state (MeOBP(T₁)) (state **b**). MeOBP(T₁) abstracts the hydrogen from the coexisting hydrogen donors (2-propanol in the present study) to form the ketyl radical (MeOBPH•) (state **c**).^{21,31–35} Although MeOBPH• cannot reduce *N*-methylphthalimide (MePI), the excited MeOBPH• (MeOBPH•(D₁)) can reduce MePI. The MeOBPH•(D₁) (state **d**) generated by excitation by the VIS laser reduces the MePI moiety to form the diphenylmethanol cation and MePI radical anion (MePI•⁻) (state **e**). The diphenylmethanol cation quickly deprotonates to regenerate MeOBP (state **f**). In the presence of an appropriate electron acceptor, the formed MePI•⁻ reduces the acceptors to regenerate the initial state **a**. As a result, a circular reaction is completed. The formed MePI•⁻ showed long lifetime (*ca.* 60 μs in acetonitrile) in the absence of acceptors, inferring that there is no serious consuming process of MePI•⁻ inhibiting the photosensitized reduction of acceptors.²¹

A crucial process of the cycle is the formation of byproduct through the coupling of radicals. However, the fixing of RP on the substrate limits the diffusion of radicals, resulting in the suppression of the formation of photochemical byproducts. When the RP is coordinated on the Si wafer and irradiated with UV and VIS light in the presence of hydrogen donor, the RP repeatedly sensitizes to reduce Ag ion to generate Ag⁰ at the solid–liquid interface.

Materials

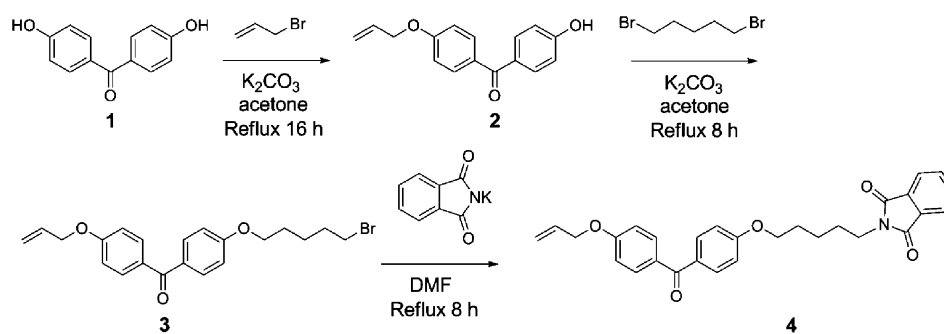
4,4'-Dihydroxybenzophenone (**1**), allyl bromide, 1,5-dibromopentane, potassium carbonate, (3-mercaptopropyl)trimethoxysilane (MPTMS) and sulfuric acid were purchased from Sigma-Aldrich and used without purification. Acetone, *N,N*-dimethylformamide (DMF), dichloromethane, hexane, *n*-octane, chloroform, sodium sulfate and potassium phthalimide were purchased from Wako and used as received. Dithiothreitol (DTT), and hydrogen peroxide was purchased from Nacalai. 2,2'-Azobis(isobutyronitrile) (AIBN) was purchased from TCI. Si wafers were purchased from SUMCO.

Synthesis of organic compound 4

The overall synthesis leading to compound **4** is shown in Scheme 2.

Compound 2. Compound **1** (18.7 mmol) and allyl bromide (18.7 mmol) were dissolved in acetone (50 ml) and stirred for 10 min at room temperature. K₂CO₃ (20.2 mmol) was added to the solution and refluxed for 16 h.³⁶ The reaction mixture was diluted with water (100 ml), extracted with CH₂Cl₂, dried with anhydrous Na₂SO₄, filtered, concentrated *in vacuo*, and separated by column chromatography (silica gel, 230–400 mesh) using CH₂Cl₂ and CH₂Cl₂–acetone (15 : 1, v/v) to give **2** in 26% yield. ¹H NMR spectra (CDCl₃), δ 7.78 (4H), 6.97 (4H), 6.07 (1H), 5.44 (1H), 5.33 (1H), 4.62 (2H). FAB mass, *m/z*: calc. 254.285, found 255.

Compound 3. Compound **2** (6.66 mmol) and 1,5-dibromopentane (66.6 mmol) were dissolved in acetone (60 ml) and stirred for 10 min at room temperature. K₂CO₃ (7.19 mmol) was added to the solution with stirring at room temperature and refluxed for 8 h. Water (100 ml) was added to the reaction mixture which was then extracted with CH₂Cl₂. The organic phase was dried over anhydrous Na₂SO₄, filtered, evaporated *in vacuo* and separated by column chromatography using hexane, hexane–CH₂Cl₂ (3 : 1, v/v), CH₂Cl₂



Scheme 2 Overall synthesis of compound 4.

and CH_2Cl_2 -acetone (15:1, v/v) to give **3** in 87% yield. ^1H NMR spectra (CDCl_3), δ 7.56 (4H), 6.96 (4H), 6.06 (1H), 5.44 (1H), 5.31 (1H), 4.61 (2H), 4.05 (2H), 3.46 (2H), 1.94 (2H), 1.83 (2H), 1.65 (2H). FAB mass, m/z : calc. 403.315, found 404.

Compound 4. To a solution of **3** (2.48 mmol) in DMF (50 ml), potassium phthalimide (2.69 mmol) was added in portions with stirring at room temperature and the reaction mixture was refluxed for 8 h. This was poured into water (100 ml), extracted with CH_2Cl_2 , dried over anhydrous Na_2SO_4 , filtered, evaporated *in vacuo*, and separated by column chromatography (hexane and CH_2Cl_2) to give **4** in 79% yield. ^1H NMR (CDCl_3), δ 7.82 (2H), 7.74 (6H), 6.96 (4H), 6.06 (1H), 5.44 (1H), 5.32 (1H), 4.62 (2H), 4.04 (2H), 3.73 (2H), 1.87 (2H), 1.78 (2H), 1.56 (2H). FAB mass, m/z : calc. 469.536, found 470.

Preparation of RP-coordinated Si wafers

The preparation of RP-coordinated Si wafers is schematically shown in Scheme 3.

(i) Si wafers were placed in Piranha solution (H_2SO_4 - H_2O_2 = 1:3, v/v, 200 ml) and heated at 90 °C for 30 min and then cooled to room temperature. The cleaned Si wafers were then immediately rinsed by Milli-Q water and stored in Milli-Q water until use.³⁷

(ii) To form the MPTMS monosurface on the Si wafer, the cleaned Si wafers were placed in an *n*-octane solution of MPTMS (5 mM) and allowed to stand at room temperature

for 24 h under Ar atmosphere.³⁷ For the fabrication of a surface composed of mixed organic molecules (MPTMS-trimethoxy(propyl)silane (TMPS) = 1:10, v/v), the cleaned Si wafers were placed in an *n*-octane solution of a mixture of MPTMS (0.5 mM) and TMPS (5 mM) and allowed to stand at room temperature for 24 h under Ar atmosphere. The formation of a planar organic surface on the Si wafer was confirmed by atomic force microscopy (AFM) (see ESI†).

(iii) The Si wafers were washed by Milli-Q water and then heated at 90 °C under Ar atmosphere. Samples were placed in a vial containing Ar-purged dithiothreitol (DTT) aqueous solution for 30 min. In a flask, **4** (205 mM) and 2,2'-azobis(isobutyronitrile) (AIBN) (10 mg) were added to CHCl_3 (200 ml) and stirred for 10 min. The MPTMS modified Si wafer was then placed into this solution and refluxed (65 °C) for 14 h. After cooling to room temperature, the RP-coordinated Si wafers (substrate **I**) were rinsed with CHCl_3 and acetone. We confirmed that the coupling reaction proceeds in high yield (80%) in solution (see ESI†). The formation of a planar organic surface on the Si wafer was confirmed by AFM (see ESI†).

Two-colour two-laser irradiation set-up

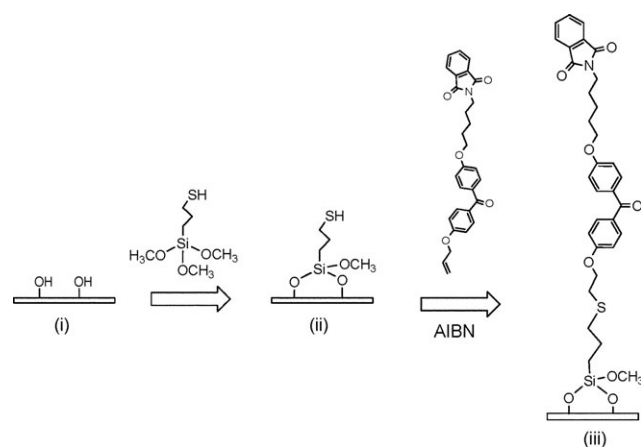
The two-colour two-laser irradiation was carried out using an Ar ion laser operating at 363.8 nm (Spectra Physics, BeamLok®2065) as the UV laser and an Ar ion laser operating at 514.5 nm (Spectra Physics, BeamLok®2060-4S) as the VIS laser.

Set-up for the photosensitized reduction of Ag ions on the substrate

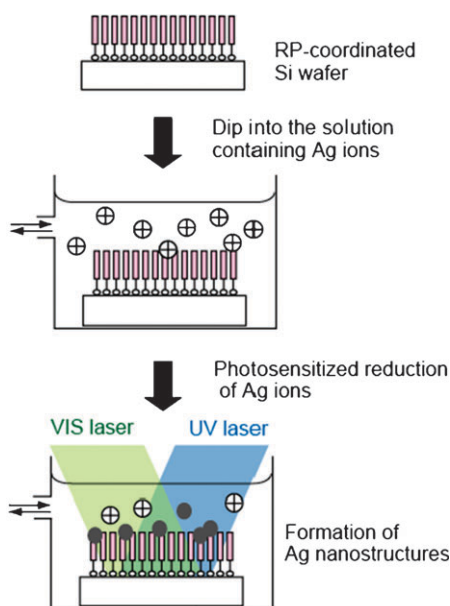
The set-up for the photosensitized reduction of Ag ions on the substrate is shown in Scheme 4. The substrate was set in a quartz cuvette filled with an aqueous alcoholic solution of AgNO_3 . The AgNO_3 solution in the cuvette was replaced slowly using the pump. The UV and VIS lasers having wavelengths of 363.8 and 514.5 nm, respectively, were operated simultaneously to overlap the two laser beams on the substrate.

Scanning electron microscopy

SEM imaging was carried out on a Hitachi S-5200 type SEM equipped with a field emission gun at an acceleration voltage of 5 kV. EDS mapping and elemental analysis were carried out



Scheme 3 Preparation of RP-coordinated Si wafers.



Scheme 4 Schematic illustration of the experimental procedure for the photosensitized fabrication of Ag nanostructures on the organic surface of the substrate.

using an EDAX Genesis XM2 EDS analysis system at an acceleration voltage of 5 kV.

Transmission electron microscopy

A poly(vinyl acetate) (PVAc) film was fabricated on the double laser beam-irradiated organic surface by casting an acetonitrile solution of PVAc (10 wt%) on the surface. The PVAc film on the organic surface was then carefully peeled off and dissolved in acetone and the solution was cast on the carbon coated TEM grid. During the processes, the Ag nanostructures on the organic surface were moved to the TEM grid. TEM images were obtained using a Hitachi H-9000 TEM equipped with a tilting device and operated at 300 kV. The images were recorded under axial illumination by a CCD camera (model XR-100 by AMT).

Results

The Si wafer containing attached coordinated recyclable photosensitizer (RP) (substrate I) was placed in an aqueous 2-propanol solution (ratio of 2-propanol to water, $R_{2\text{-pro/water}} = 1:4$, v/v, dielectric constant, $\epsilon_{\text{mix}} = 68$; 2-propanol acts as a hydrogen donor)³⁸ of AgNO_3 (1 mM), and then, UV and VIS lasers having wavelengths of 363.8 and 514.5 nm, respectively, were irradiated to overlap the two laser beams on the substrate I (Scheme 4). Due to the concomitant irradiation of the two-colour laser beams, the RP reduces the Ag ions to generate Ag atoms (the mechanism is described in the Experimental section).²¹ After the irradiation by the lasers for 2 h, the substrate I was removed from the solution and carefully washed using Milli-Q water. Since the absorption of solution after the photoirradiation does not show the surface plasmon band of the Ag nanostructure, most Ag atoms would be generated in the neighborhood of the substrate and form nanostructures at the interface.

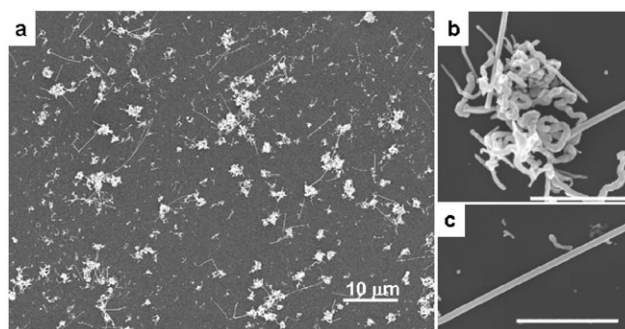


Fig. 1 (a) SEM image of Ag nanostructures fabricated on substrate I during irradiation by two-colour laser beams (2 h) in aqueous alcoholic solution ($\epsilon_{\text{mix}} = 68$) of AgNO_3 (1 mM). (b) Entangled Ag nanowire. Scale bar is 1 μm . (c) Straight nanowire. Scale bar is 1 μm .

Fig. 1 shows SEM images of substrate I after irradiation by the lasers. Two types of nanostructures were observed on the substrate. One type was nanoparticles having diameters of several tens of nanometers, while the other type was in the form of sparsely distributed nanowires having diameters of 30–100 nm. The Ag nanowires consisted of entangled and straight regions. The elemental map indicated that the nanowires were composed of Ag (see ESI,[†] Fig. S1). The TEM images and electron diffraction (ED) pattern of a typical Ag nanowire are shown in Fig. 2. A selected area ED pattern indicated that the straight region consisted of a single crystal having *fcc* Ag structure grown along the $\langle 111 \rangle$ direction.

When a (3-mercaptopropyl)trimethoxysilane (MPTMS)-coordinated Si wafer (*i.e.*, a substrate without RP) was treated under the similar conditions, no nanostructures were formed while when a single UV laser was used for the irradiation, the nanowires formed were much shorter than those formed when two-colour laser beams were used (see ESI,[†] Fig. S3).³⁹ These facts indicate that the Ag nanostructures on the substrate I were generated due to the photosensitization by the RP. Although the ketyl radical generated by the single UV laser would also reduce the Ag ions, this process is ineffective.^{12,39–42}

One of the important factors that determines the crystal morphology at the solid–liquid interface is the interactions between the substrate, solution and crystal phases. When crystals are completely wetted on the substrate, the crystals

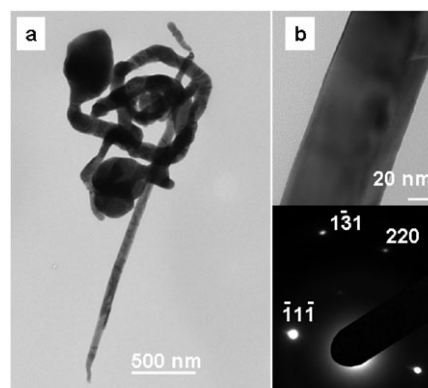


Fig. 2 (a) TEM image of an entire Ag nanowire. (b) Enlarged image of straight part and corresponding selected area ED pattern.

form a film on the substrate because the surface free energy decreases due to the direct bonding of the crystal on the substrate. On the contrary, when the substrate is incompletely wetted, crystals form three-dimensional (3-D) islands. In the case of incomplete wetting, heterogeneous nucleation is not observed on the substrate.

To investigate the effect of the interactions between the substrate, solution and crystal phases, we attempted to fabricate a Ag nanostructure in a less-polar solution (ratio of 2-propanol to water, $R_{2\text{-pro/water}} = 4:1$, v/v, dielectric constant ($\epsilon_{\text{mix}} = 32$)). The contact angles (θ) of the polar ($\epsilon_{\text{mix}} = 68$) and less polar ($\epsilon_{\text{mix}} = 32$) solutions on substrate **I** were estimated to be 30° and $<5^\circ$, respectively (see ESI†). The less polar solvent showed much better affinity for the substrate **I**.

A change in the solvent polarity resulted in a dramatic change in the morphology of the nanostructure. While nanowires were formed in the polar solution, nanoplates were formed in the less polar solution (Fig. 3 and ESI,† Fig. S5). Ag nanoparticles with diameters of several tens of nanometers were also observed. The width of the nanoplates were 50–100 nm and heights were 30–50 nm. Elemental analysis confirmed that the nanoplates were composed of Ag (see ESI,† Fig. S2). TEM images and selected area ED pattern of a nanoplate are shown in Fig. 4. The ED pattern indicated that the primary face of the Ag nanoplate was of $\langle 111 \rangle$ -type. The faint spots of ED patterns within the $\langle 220 \rangle$ spots are assigned to be the $1/3 \langle 422 \rangle$ spots. These spots are not observed in the single-crystal *fcc* metal; however, these spots can appear when the twin planes are parallel to each other.^{43–45} A similar ED pattern was observed in Ag nanotriangles and plates in previous reports.^{43–45}

Discussion

Formation mechanisms of nanowires

In this section, we discuss the formation mechanism of nanostructures and the role of the solid–liquid interface during the formation. In order to further investigate the formation mechanism of nanostructures, we observed the growth process of nanowires at different laser irradiation times (Fig. 5). After 10-min laser irradiation in the polar solution, Ag nanoparticles having diameters of 6 ± 3 nm were formed, and no anisotropic structures were observed. Larger nanoparticles having diameters

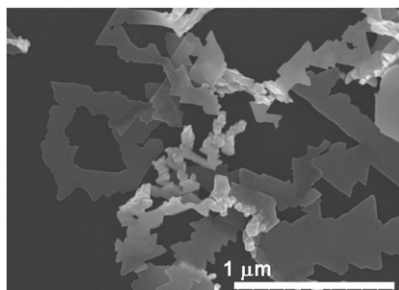


Fig. 3 SEM image of Ag nanoplates fabricated on substrate **I** during irradiation by two-colour laser beams (2 h) in aqueous alcoholic solution ($\epsilon_{\text{mix}} = 32$) of AgNO_3 (1 mM).

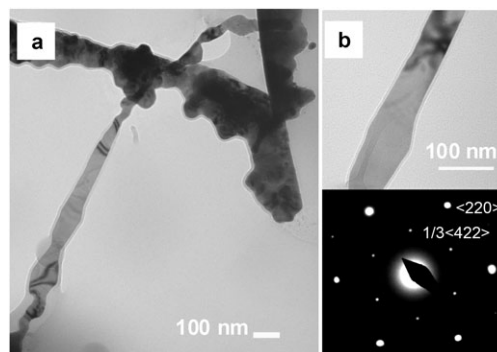


Fig. 4 (a) TEM image of Ag nanoplates. (b) Enlarged image of Ag nanoplates and corresponding selected area ED pattern.

of approximately 100 nm were also observed as a minor component. Anisotropic structures (*i.e.*, nanorod-like structures and short nanowires) were observed after 30-min laser irradiation. The nanowires grew larger and longer with further irradiation. With regard to the surface of the nanowires, it was observed that a number of small nanoparticles were attached to the surface. This observation suggested that the attachments and fusion of small nanoparticles on the nanowire's surface is a process of nanowire growth. Nanowires, like those shown in Fig. 1, were formed after laser irradiation for 2 h.

Next, we tried to investigate the effect of interaction between the Ag crystal phase and different substrates. A mixed substrate was prepared from trimethoxy(propyl)silane (TMPS) and RP (TMPS:RP = 10:1, v/v) (substrate **II**) and Ag nanostructures were fabricated on this surface (Fig. 6(a)). Interestingly, only polygonal structures were observed on substrate **II**. This result implies that the interaction between solvent molecules and the crystal phase was not responsible for the nanowire formation. In addition, since the θ value of the polar solution ($\epsilon_{\text{mix}} = 68$) on substrate **II** (30°) was close to that on substrate **I** (32°), it was assumed that the interaction between the organic surface and the solution was also not responsible for the change in morphology of the nanostructure. The carbonyl group of the RP was assumed to interact with the Ag clusters.⁴⁶ The concentration of the carbonyl group on substrate **II** was smaller than that on substrate **I**; therefore, the interaction of substrate **II** with the Ag crystal phase should be weak. These facts imply that the interaction of the Ag crystal phase with the surface organic molecules were responsible for the growth of anisotropic structures.

Taking the above results into account, there would be two growing processes of Ag nanowires. The first is the anisotropic growth of single crystal. Since the interfacial free energy of $\langle 111 \rangle$ is smaller than that of $\langle 100 \rangle$ and $\langle 110 \rangle$ for *fcc* structures, the growth rate along the closed-packed $\langle 111 \rangle$ direction is faster than that along other directions.^{47–49} The difference of the crystal growth rate would be a reason for the formation of Ag nanowire grown along the $\langle 111 \rangle$ direction.

It is assumed that slow reduction rate is an important factor for the nanowire formation because the high concentration of Ag nuclei is unfavorable for the anisotropic crystal growth.^{50,51} In the polar solution, the concentration of the hydrogen donor (2-propanol) is one-quarter of that in the less

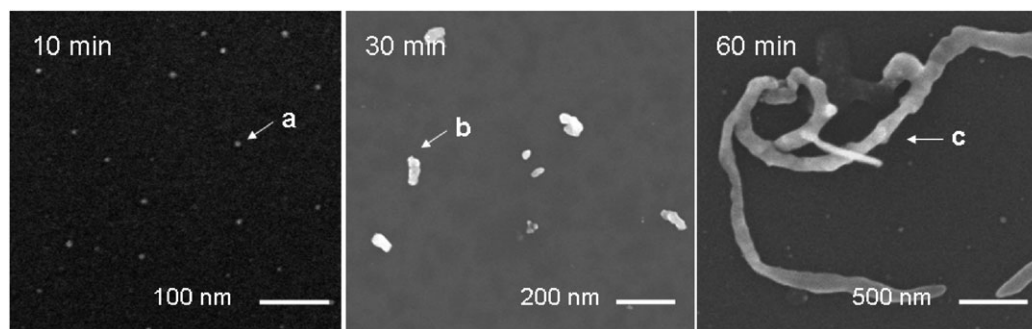


Fig. 5 Typical Ag nanostructures on substrate **I** after irradiation by two-colour laser beams for 10, 30 and 60 min in polar solution ($\epsilon_{\text{mix}} = 68$) of AgNO_3 (1 mM). (a) Nanoparticles having diameter of 6 ± 3 nm, (b) nanorod-like structure and (c) short nanowire. For the nanowire in (c) it was observed that a number of small nanoparticles were attached to the surface.

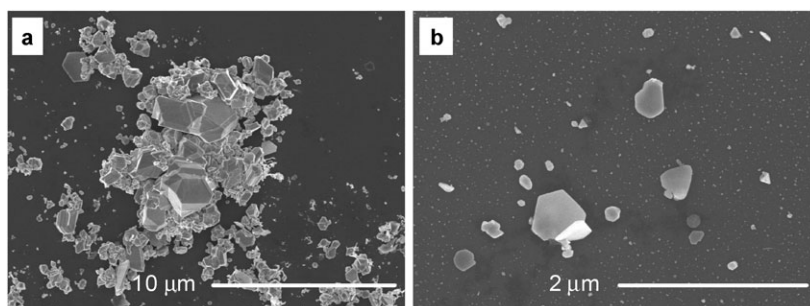


Fig. 6 SEM image of Ag nanostructures fabricated on substrate **II** in (a) polar and (b) less polar solution during irradiation by two-colour laser beams (2 h).

polar solution. In addition, the hydrogen abstraction ability of benzophenone decreases with increasing solvent polarity.⁵² These facts infer that the rate of photochemical reduction of Ag ions in the polar solvent is sufficiently slow to allow the anisotropic crystal growth.

The attachment and fusion of small nanoparticles on the surface of the nanowires are alternative processes of nanowire growth. The change in the morphology of the nanostructure depending on the substrate used indicates that the interaction between Ag crystals and the surface organic molecule (*i.e.* RP) supports anisotropic growth. The anisotropic crystal growth and nanoparticle attachment assisted by the RP promote the formation of nanowires.

Formation mechanisms of nanoplates

Fig. 7 shows the growth process of Ag nanoplates in the less polar ($\epsilon_{\text{mix}} = 32$) solution. After 10-min laser irradiation, nanotriangles and nanoparticles with broad size distributions were formed. Further irradiation reduced the number of nanoparticles formed; in addition, the nanotriangles evolved into short nanoplates.

These observations indicate that nanoplates are formed by a two-step process: (i) the formation of nanotriangles and (ii) the evolution of nanotriangles into nanoplates. The VIS light-induced conversion of nanoparticles to nanotriangles is a well-known process.^{44,45} To analyze the effect of a VIS laser, we fabricated Ag nanostructures using a single UV laser. When a single UV laser was used for the irradiation, few nanoparticles and aggregates were formed (see ESI,† Fig. S4). This fact indicates that the VIS laser is required for the

generation of nanoplates. The VIS laser irradiation digests the nanoparticles into smaller seeds to form the nanotriangles, which then grew into the nanoplates.^{43,44}

The temporal transition of the size distribution of nanostructures on the substrate (*i.e.*, decrease in the number of smaller nanostructures and increase in the number of larger ones) is typical in the Ostwald ripening process (Fig. 8). Thus the Ag nanotriangles formed evolved into nanoplates through the Ostwald ripening process. Taking the result of ED analysis of Ag nanoplates into account, it is assumed that the twin planes of the Ag nanotriangles play an important role in the formation of plate-like nanostructures. The re-entrant grooves of the faces of the twin planes cause the rapid growth of the nanostructures leading to the formation of larger triangles or anisotropic structures (*i.e.* Ag plates).⁴³

Although a change of the substrate from **I** to **II** caused a dramatic change in the morphology of the nanostructure in a polar ($\epsilon_{\text{mix}} = 68$) solution, no significant morphological change was observed when the substrate was changed in the less polar ($\epsilon_{\text{mix}} = 32$) solution (Fig. 6(b)). As shown in Fig. 6(b), premature nanoplate structures were observed on substrate **II**. These structures had a similar ED pattern to that of the nanoplates (data not shown). The ineffective growth of the nanostructures on substrate **II** compared with that on substrate **I** can be attributed to the lower concentration of RP. It seems that the important factor responsible for the nanoplate formation is the formation process itself rather than the interaction between the crystal phase and the substrate.

In the case of aqueous alcoholic solutions of Ag^0 , the decrease of solvent polarity would decrease the degree of

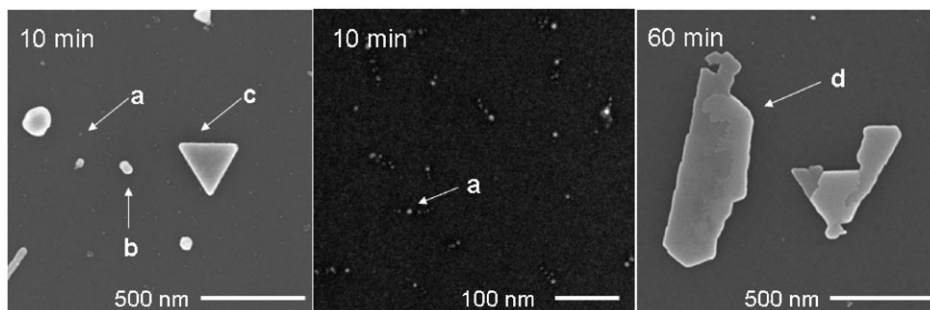


Fig. 7 Ag nanocrystals generated on substrate **I** after irradiation by two-color laser beams for 10 and 60 min in less polar solution ($\epsilon_{\text{mix}} = 32$) of AgNO_3 . (a) Nanoparticle having a diameter smaller than 10 nm (the average diameter is 5 ± 4 nm), (b) larger nanoparticle having a diameter of approximately 100 nm, (c) nanotriangle and (d) short nanoplate.

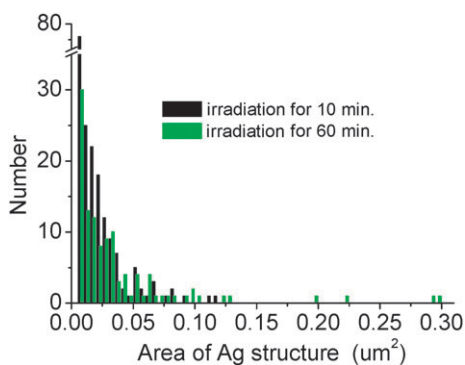


Fig. 8 The temporal evolution of size distribution of Ag nanostructures in less polar solution. Since the shape of structures is complicated, the size was expressed by the area. As laser irradiation progressed, the number of small nanostructures ($< 0.03 \mu\text{m}^2$ in area) decreased, while the number of large nanostructures ($0.2\text{--}0.3 \mu\text{m}^2$ in area) increased.

supersaturation and the critical nucleus size increases with decreasing the degree of supersaturation. Since the nuclei having sizes smaller than the critical nucleus size are unstable and spontaneously dissolve in the solution, nanostructure growth by the Ostwald ripening process is preferable in a solution with a low degree of supersaturation (*i.e.*, less polar solution). Furthermore, the formation of Ag nanotriangles in the less polar solution implies that the irradiation of the VIS laser digests the Ag nanoparticles to smaller Ag clusters.^{44,45} This digestion of Ag nanoparticles would enhance the Ostwald-ripening-like process.

Conclusions

In this study, we successfully fabricated Ag nanostructures at the solid–liquid interface using a recyclable photosensitization system and investigated the morphology of the formed nanostructures. It was demonstrated that the recyclable photosensitization is a useful method to fabricate various metal nanostructures at the solid–liquid interfaces.

The morphology of the generated Ag nanostructures was dependent on the type of substrate used and the solvent polarity. The formation of Ag nanowires in a polar solvent is assisted by the interactions between the Ag crystal phase and organic molecules on the substrate. On the other hand,

light-induced shape variation and the crystal growth by the Ostwald ripening process become pronounced in a less polar solvent leading to the formation of Ag nanotriangles, which ultimately evolve into nanoplates.

The present photochemical approach can apply various solvents and surface-modified substrates. A better understanding of the factors that determine the morphology of nanostructures would enable us to develop better means to control the morphology of nanostructures at the solid–liquid interface.

Acknowledgements

This work has been partly supported by a Grant-in-Aid for Scientific Research (Project 17105005, 19710094, and others) from the Ministry of Education, Culture, Sports, Science and Technology (MEXT) of Japanese Government. TEM and SEM observations were supported by “Nanotechnology Network Project of MEXT, Japan” at Research Center for Ultrahigh Voltage Electron Microscopy, Osaka University (Handai Multi-functional Nano-Foundry).

Notes and references

- 1 S. Link and M. A. El-Sayed, *J. Phys. Chem. B*, 1999, **103**, 8410.
- 2 D. D. Evanoff, Jr. and G. Chumanov, *ChemPhysChem*, 2005, **6**, 1221.
- 3 A. L. Pyayt, B. Wiley, Y. Xia, A. Chen and L. Dalton, *Nat. Nanotechnol.*, 2008, **3**, 660.
- 4 P. K. Jain, X. Huang, I. H. El-Sayed and M. A. El-Sayed, *Acc. Chem. Res.*, 2008, **41**, 1578.
- 5 I. Pastoriza-Santos and L. M. Liz-Marzán, *J. Mater. Chem.*, 2008, **18**, 1724.
- 6 V. Amendola and M. Meneghetti, *Phys. Chem. Chem. Phys.*, 2009, **11**, 3805.
- 7 C. R. Martin, *Science*, 1994, **266**, 1961.
- 8 B. L. Cushing, V. L. Kolesnichenko and C. J. O'Connor, *Chem. Rev.*, 2004, **104**, 3893.
- 9 C. Burda, X. Chen, R. Narayanan and M. A. El-Sayed, *Chem. Rev.*, 2005, **105**, 1025.
- 10 J. A. Dahl, B. L. S. Maddux and J. E. Hutchison, *Chem. Rev.*, 2007, **107**, 2228.
- 11 Y. Xia, Y. Xiong, B. Lim and S. E. Skrabalak, *Angew. Chem., Int. Ed.*, 2009, **48**, 60.
- 12 M. Sakamoto, M. Fujitsuka and T. Majima, *J. Photochem. Photobiol., C*, 2009, **10**, 33.
- 13 M. Sakamoto, T. Tachikawa, M. Fujitsuka and T. Majima, *Langmuir*, 2009, DOI: 10.1021/la901552f.
- 14 M. Sakamoto, T. Tachikawa, M. Fujitsuka and T. Majima, *J. Am. Chem. Soc.*, 2009, **131**, 6.

- 15 M. Sakamoto, T. Tachikawa, M. Fujitsuka and T. Majima, *Adv. Mater.*, 2008, **20**, 3427.
- 16 M. Sakamoto, T. Tachikawa, M. Fujitsuka and T. Majima, *Chem. Mater.*, 2008, **20**, 2060.
- 17 M. Sakamoto, T. Tachikawa, M. Fujitsuka and T. Majima, *Adv. Funct. Mater.*, 2007, **17**, 857.
- 18 M. Sakamoto, T. Tachikawa, S. S. Kim, M. Fujitsuka and T. Majima, *ChemPhysChem*, 2007, **8**, 1701.
- 19 M. Sakamoto, T. Tachikawa, M. Fujitsuka and T. Majima, *Langmuir*, 2006, **22**, 6361; erratum: M. Sakamoto, T. Tachikawa, M. Fujitsuka and T. Majima, *Langmuir*, 2007, **23**, 7886.
- 20 M. Sakamoto, T. Tachikawa, M. Fujitsuka and T. Majima, *Chem. Phys. Lett.*, 2006, **420**, 90; erratum: M. Sakamoto, T. Tachikawa, M. Fujitsuka and T. Majima, *Chem. Phys. Lett.*, 2007, **442**, 170.
- 21 M. Sakamoto, S. S. Kim, M. Fujitsuka and T. Majima, *J. Phys. Chem. C*, 2007, **111**, 6917.
- 22 J. Aizenberg, A. J. Black and G. M. Whitesides, *Nature*, 1999, **398**, 495.
- 23 J. Aizenberg, A. J. Black and G. M. Whitesides, *J. Am. Chem. Soc.*, 1999, **121**, 4500.
- 24 J. Aizenberg, *Adv. Mater.*, 2004, **16**, 1295.
- 25 A. L. Briseno, J. Aizenberg, Y.-J. Han, R. A. Penkala, H. Moon, A. J. Lovinger, C. Kloc and Z. Bao, *J. Am. Chem. Soc.*, 2005, **127**, 12164.
- 26 R. Turgeman, O. Gershevit, M. Deutsch, B. M. Ocko, A. Gedanken and C. N. Sukenik, *Chem. Mater.*, 2005, **17**, 5048.
- 27 R. M. Penner, *Acc. Chem. Res.*, 2000, **33**, 78.
- 28 S.-J. Huo, X.-K. Xue, Q.-X. Li, S.-F. Xu and W.-B. Cai, *J. Phys. Chem. B*, 2006, **110**, 25721.
- 29 J. W. P. Hsu, W. M. Clift and L. N. Brewer, *Langmuir*, 2008, **24**, 5375.
- 30 N. A. J. M. Sommerdijk and G. de With, *Chem. Rev.*, 2008, **108**, 4499.
- 31 M. Sakamoto, X. Cai, S. S. Kim, M. Fujitsuka and T. Majima, *J. Phys. Chem. A*, 2007, **111**, 223.
- 32 M. Sakamoto, X. Cai, M. Fujitsuka and T. Majima, *J. Phys. Chem. A*, 2006, **110**, 11800.
- 33 M. Sakamoto, X. Cai, M. Fujitsuka and T. Majima, *Chem.–Eur. J.*, 2006, **12**, 1610.
- 34 M. Sakamoto, X. Cai, M. Fujitsuka and T. Majima, *J. Phys. Chem. A*, 2005, **109**, 6830.
- 35 M. Sakamoto, X. Cai, M. Hara, S. Tojo, M. Fujitsuka and T. Majima, *J. Phys. Chem. A*, 2004, **108**, 8147.
- 36 O. Prucker, C. A. Naumann, J. Ruhe, W. Knoll and C. W. Frank, *J. Am. Chem. Soc.*, 1999, **121**, 8766.
- 37 S. R. Wasserman, Y. T. Tao and G. M. Whitesides, *Langmuir*, 1989, **5**, 1074.
- 38 The dielectric constant of the mixed solvent was calculated based on the equation: $\epsilon = \epsilon_{\text{water}}x_{\text{water}} + \epsilon_{2\text{pro}}x_{2\text{pro}}$.
- 39 Nanowires were formed even when the VIS laser was not used; this indicated that the VIS laser is not essential for the formation of nanowires. However, VIS laser much enhanced the formation efficiency of Ag nanoparticles and wires on the surface. Since the oxidation potential of ketyl radical (-0.25 V vs. SCE) is less negative than that of MePI $^{\bullet-}$ (-1.37 V vs. SCE) generated by the two-colour two-laser excitation, the reduction efficiency of Ag ion was much enhanced under the two-colour two-laser irradiation (see ref. 21).
- 40 A. Henglein, *Chem. Mater.*, 1998, **10**, 444.
- 41 Y. Yonezawa, T. Sato, S. Kuroda and K. Kuge, *J. Chem. Soc., Faraday Trans.*, 1991, **87**, 1905.
- 42 N. Kometani, H. Doi, K. Asami and Y. Yonezawa, *Phys. Chem. Chem. Phys.*, 2002, **4**, 5142.
- 43 C. Lofton and W. Sigmund, *Adv. Funct. Mater.*, 2005, **15**, 1197.
- 44 R. Jin, Y. Cao, C. A. Mirkin, K. L. Kelly, G. C. Schatz and J. G. Zheng, *Science*, 2001, **294**, 1901.
- 45 Y. Sun, B. Mayers and Y. Xia, *Nano Lett.*, 2003, **3**, 675.
- 46 I. Rabin and W. Schulze, *J. Phys. Chem. B*, 2004, **108**, 14575.
- 47 L. D. Ruslan and B. L. Brian, *Phys. Rev. Lett.*, 2005, **94**, 086102.
- 48 B. B. Laird and R. L. Davidchack, *J. Phys. Chem. B*, 2005, **109**, 17802.
- 49 S. Sun, D. Yang, D. Villers, G. Zhang, E. Sacher and J.-P. Dodelet, *Adv. Mater.*, 2008, **20**, 571.
- 50 A. I. Bhatt, A. Mechler, L. L. Martin and A. M. Bond, *J. Mater. Chem.*, 2007, **17**, 2241.
- 51 A. R. Roosen and W. C. Carter, *Phys. A*, 1998, **261**, 232.
- 52 J. C. Scaiano, *J. Photochem.*, 1974, **2**, 81.